Journal of Medicinal Chemistry

Article

pubs.acs.org/jmc

Optimization of Allosteric With-No-Lysine (WNK) Kinase Inhibitors and Efficacy in Rodent Hypertension Models

Ken Yamada,[*,†,§,#] Julian Levell,[†,#,∥] Taeyong Yoon,[†,#,⊥] Darcy Kohls,[†,#] David Yowe,[†] Dean F. Rigel,[‡,□] Hidetomo Imase,[†] Jun Yuan,[†] Kayo Yasoshima,[†,§] Keith DiPetrillo,[‡,▽] Lauren Monovich,[†] Lingfei Xu,[‡] Meicheng Zhu,[†,○] Mitsunori Kato,[†,§] Monish Jain,[†] Neeraja Idamakanti,[†,◆] Paul Taslimi,[†,⬢] Toshio Kawanami,[†,§] Upendra A. Argikar,[†] Vidya Kunjathoor,[†] Xiaoling Xie,[†] Yukiko I. Yagi,[§,¶] Yuki Iwaki,[†,△] Zachary Robinson,[†,▼] and Hyi-Man Park[†,§,#]

[†]Novartis Institutes for BioMedical Research, Inc., Cambridge, Massachusetts 02139-4133, United States

[‡]Novartis Institutes for BioMedical Research, Novartis Pharmaceuticals Corporation, East Hanover, New Jersey 07936-1080, United States

[§]Novartis Institutes for BioMedical Research, Novartis Pharma K.K., Tsukuba, Ibaraki 300-2611, Japan

Supporting Information

ABSTRACT: The observed structure−activity relationship of three distinct ATP noncompetitive With-No-Lysine (WNK) kinase inhibitor series, together with a crystal structure of a previously disclosed allosteric inhibitor bound to WNK1, led to an overlay hypothesis defining core and side-chain relationships across the different series. This in turn enabled an efficient optimization through scaffold morphing, resulting in compounds with a good balance of selectivity, cellular potency, and pharmacokinetic profile, which were suitable for *in vivo* proof-of-concept studies. When dosed orally, the optimized compound reduced blood pressure in mice overexpressing human WNK1, and induced diuresis, natriuresis and kaliuresis in spontaneously hypertensive rats (SHR), confirming that this mechanism of inhibition of WNK kinase activity is effective at regulating cardiovascular homeostasis.

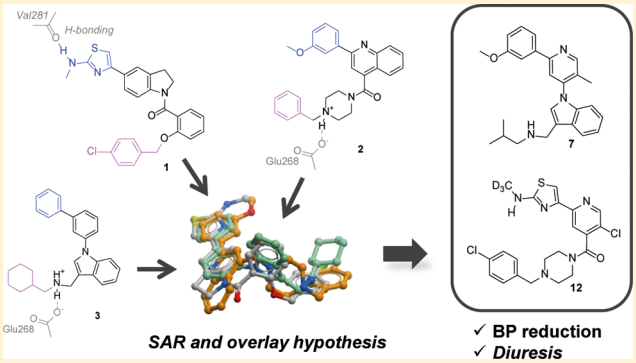

INTRODUCTION

In pseudohypoaldosteronism-II (PHAII) patients, mutations in With-No-Lysine (WNK) kinases have been described as causing hypertension with a paradoxical decrease in aldosterone, suggesting a mechanism of blood pressure regulation independent of the renin−angiotensin−aldosterone system.[1,2] We have previously shown that WNK476, a small molecule ATP-competitive inhibitor of WNK kinase catalytic activity, induces diuresis and blood pressure reduction in various rodent models of hypertension.[3] The finding was consistent with previous reports of WNK-mediated phosphorylation of oxidative-stress response 1 (OSR1) and STE20/SPS1-related proline/alanine-rich kinase (SPAK), that in turn regulate, via phosphorylation, the functions of renal electrolyte transporters such as the sodium chloride cotransporter (NCC) and the sodium potassium chloride cotransporter (NKCC1),[4−6] as well as the cellular phenotypes observed with a recently reported WNK-SPAK disruptor.[7]

Prior to the discovery of the ATP-competitive WNK476, we had identified compounds **1**, **2**, and **3** as allosteric inhibitors of WNK kinases[8] (Figure 1a). This mechanism of inhibition was thought to be advantageous vs binding in the ATP site, in terms of achieving the exquisite selectivity required to ensure safety for chronic administration as an antihypertensive agent.[9−11] Allosteric inhibition was also potentially beneficial for achieving potent efficacy in the cellular context, where ATP concentration is very high.[8] At the time, compound **1** was the only one that cocrystallized with WNK1, revealing an allosteric binding mode (Figure 1b, 5TF9). However, similar to compound **1**, both compounds **2** and **3** showed the best fit for ATP noncompetitive inhibition upon enzyme kinetic studies (Figures S1a−c). This suggested the possibility of similar allosteric inhibition across the three compounds.

In order to rationalize this observation we developed an overlay hypothesis based on docking models that we could test with structure−activity relationship (SAR) studies. Aligning the hydrophobic chlorophenyl of **1** with the benzyl of compound **2** and cyclohexylmethyl of compound **3** positioned the aminothiazole of compound **1** congruent with the methoxyphenyl of compound **2** and the terminal phenyl of the biphenyl from compound **3**. Furthermore, docking models suggested that the protonated amine of both compounds **2** and **3** can form a hydrogen bond with Glu268 (Figure 1c,d). The reverse binding

Received: May 22, 2017

DOI: 10.1021/acs.jmedchem.7b00708
J. Med. Chem. XXXX, XXX, XXX−XXX

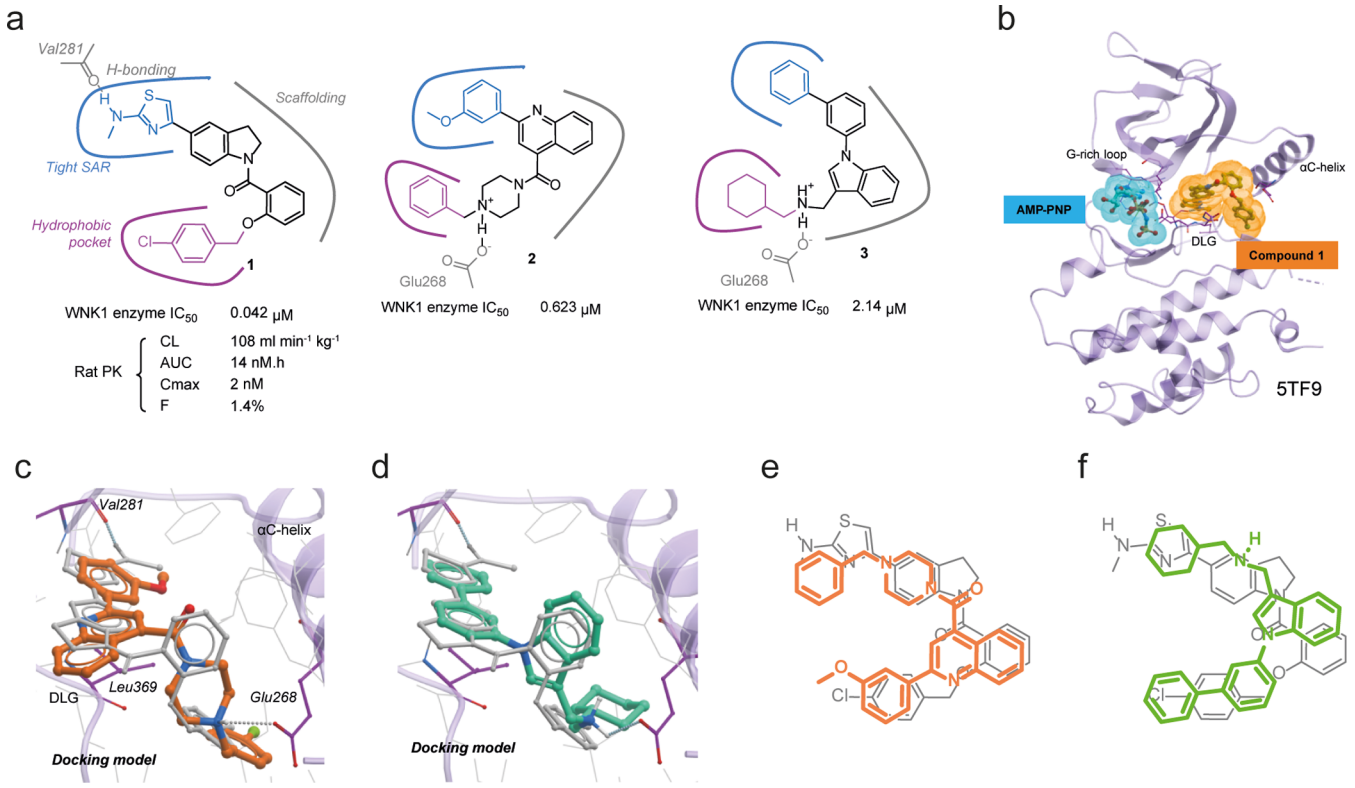

Figure 1. Summary of SAR and overlay models of three scaffolds. (a) Structures of compounds **1**−**3** and their inhibition of WNK1 kinase activity. Preliminary SAR suggested that the aminothiazole of compound **1**, methoxyphenyl of compound **2**, and phenyl of compound **3** occupy a tight pocket, whereas the chlorophenyl of compound **1**, phenyl of **2**, and cyclohexyl of compound **3** occupy a looser hydrophobic pocket. (b) Crystal structure of compound **1** (yellow) bound to WNK1 (purple) in an allosteric pocket adjacent to the ATP binding site occupied by AMP-PNP (light blue). (c) Close-up view of the binding pocket from the same angle as panel b with an overlay model of compound **2** (orange) on top of compound **1** (gray). The methoxyphenyl motif occupies the pocket occupied by the aminothiazole of compound **1**. The predicted hydrogen bonding contact of protonated amine and Glu268 is indicated as green dots. (d) Overlay model of compound **3** (green) on top of compound **1** (gray). The terminal phenyl of biphenyl motif occupies the aminothiazole pocket of compound **1**. (e) Alternative overlay of compound **2** (orange) on top of compound **1** (gray). (f) Alternative overlay of compound **3** (green) on top of compound **1** (gray).

modes for compounds **2** and **3** (Figure 1e,f) would not make the hydrogen bond contact with Glu268 and, hence, would seem less likely. Our SAR studies around compounds **1**−**3** gave a clear trend to favor the former overlay models (Figure 1c,d). Thus, a tight SAR around the methoxyphenyl group of compound **2** was observed, which was consistent with binding to the small and rigid hydrophobic pocket around the aminothiazole of compound **1** (Figure 1a). Contrary to the tight SAR for the aminothiazole or methoxyphenyl, a broader selection of hydrophobic motifs was tolerated as replacements for the chlorophenyl, phenyl, or cyclohexyl of the three compounds, suggesting that they all occupy a more flexible hydrophobic pocket and disfavor the reverse binding option for compounds **2** and **3**. Although potent, the pharmacokinetic profiles of compounds **1**, **2**, and **3** were inadequate for *in vivo* efficacy validation of this mode of WNK inhibition. Therefore, we exchanged substituents and core motifs across the three scaffolds in parallel, in order to accelerate the identification of an *in vivo* tool compound.

RESULTS AND DISCUSSION

A highly efficient optimization of compound **3** was carried out by initially engrafting the methoxy group of compound **2** to give a dramatic 60-fold improvement in potency (Figure 2a, compound **4**). Introduction of a pyridyl nitrogen to simulate the quinoline nitrogen of compound **2** gave an additional 7-fold boost in potency, most likely arising from the increased planarity. Compound **6**, a close analogue of compound **5**, with a fluoro-substituent in the 5-position of the indole was successfully cocrystallized with WNK1 (Figure 3a, PDB 5WDY). This structure confirmed the allosteric binding mode for the scaffold as well as the proposed overlay orientation of compound **2** with compound **1**. It also showed the tight pocket around the methoxyphenyl moiety as well as the proposed hydrogen bond of the protonated amine linker with Glu268. Although the poor lipophilic efficiency[12] (LipE) of compound **3** was much improved in compound **6** (−2.9 vs −0.33), we envisioned that further improvement in lipophilic efficiency through truncation of the cyclohexyl moiety would be required for a viable path forward to an *in vivo* tool compound. To this end, installation of a methyl group adjacent to the indole linkage in compound **5** introduced torsional strain to mimic the binding conformation, and this change enabled retention of potency when the cyclohexyl moiety was truncated to an isobutyl group. Compound **7** represents one of the best candidates from the series for *in vivo* proof of concept, although it still suffers from low LipE (0.12).

Many analogues of compound **2** were explored in cocrystal studies, but it was the modification of the piperazine to the (*R*)-aminopyrrolidine (Figure 2b, compound **8**), which allowed the generation of a cocrystal structure within this scaffold class, confirming the allosteric binding mode and proposed overlay

DOI: 10.1021/acs.jmedchem.7b00708
J. Med. Chem. XXXX, XXX, XXX−XXX

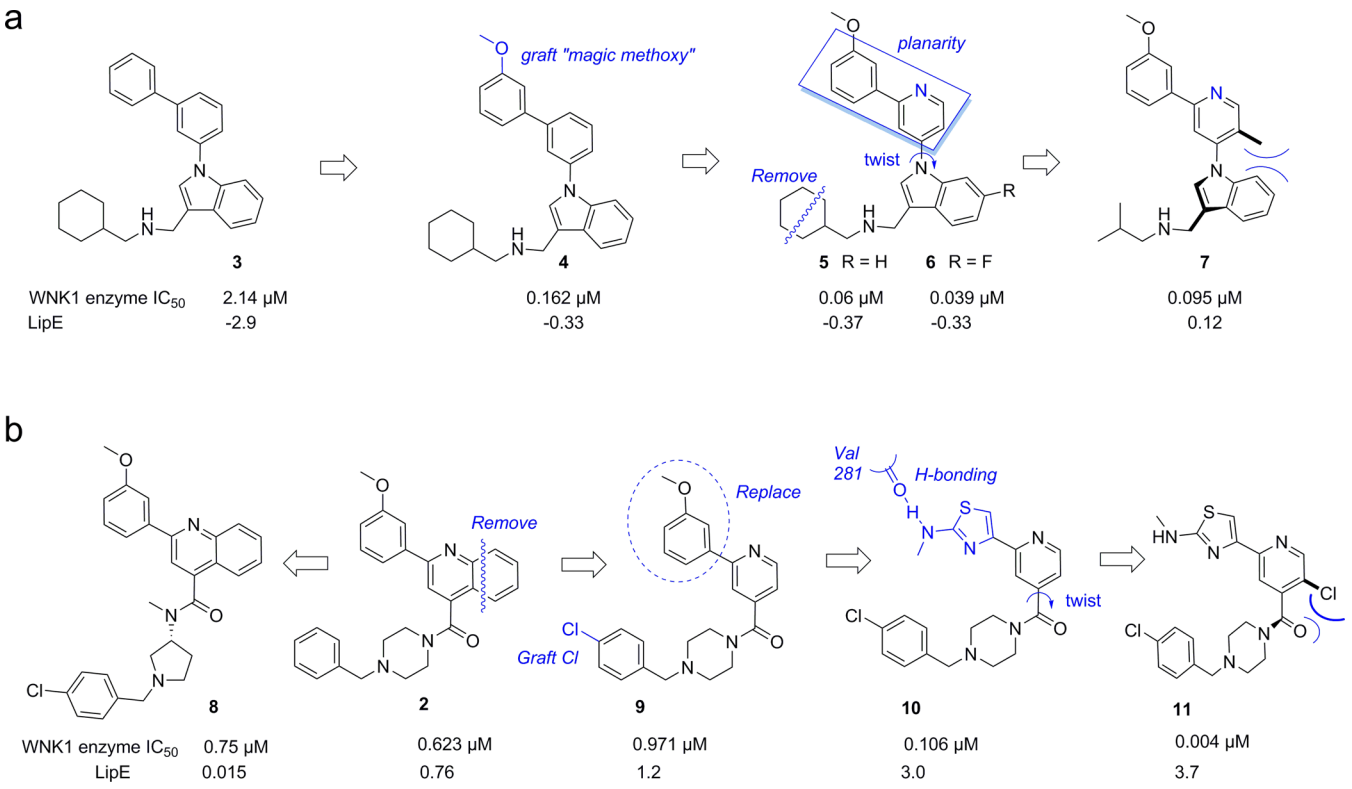

Figure 2. Morphing based optimization of the two series. (a) Introduction of methoxy to the phenyl group of compound **3** gave >100-fold improvement in potency in compound **4**, and introduction of a pyridyl nitrogen to allow for planarity gave further 4-fold improvement in potency to give compound **5**. The crystal structure with WNK1 was obtained with a fluorinated analogue compound **6**. Replacement of cyclohexyl with a simpler isobutyl group resulted in slightly less hydrophobic compound **7**, which was equipotent to compound **5**, likely owing to the introduced torsional strain. (b) Replacement of piperazine and introduction of a *para*-chloro group gave compound **8**, which was the only structure from this scaffold that cocrystallized with WNK1. Removal of the extra phenyl ring of compound **2** and installment of a *para*-chloro group gave equipotent compound **9**, whose methoxyphenyl motif was replaced with aminothiazole to give compound **10** with nearly 10-fold improvement in potency. Introduction of a chlorine substituent on the central pyridine ring gave compound **11** with a further 50-fold improvement in potency, most likely due to the introduction of torsional strain.

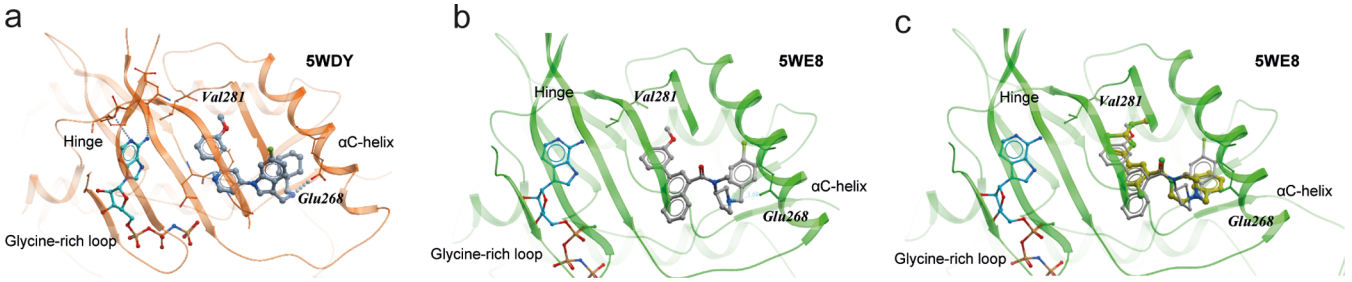

Figure 3. Allosteric binding modes of the optimized WNK inhibitors. (a) Ternary complex of compound **6** and AMP-PNP bound to WNK1, confirming the predicted orientation of binding and the hydrogen bond contact of the proton of the secondary amine with Glu268. (b) Ternary complex of compound **8** and AMP-PNP bound to WNK1, confirming the predicted orientation of binding and the hydrogen bond contact of protonated piperazine nitrogen with Glu268. (c) Docking model of compound **11** (yellow) overlaid on top of compound **8** (gray) bound to WNK1 and AMP-PNP. Confidence in the binding mode is enhanced by the crystal structures of three closely related scaffolds.

hypothesis for compound **3** vs compounds **1** and **2** (Figure 3b, PDB 5WE8). This structure also highlighted several opportunities for compound optimization. Replacement of quinoline with pyridine to simulate the biaryl of compound **3** was also supported by the lack of obvious binding interactions in the X-ray structure with this second ring system (Figure 2b). Simultaneous grafting of the *para*-chloro group from compound **1** onto the benzyl group gave compound **9** with minimal loss of potency but overall improved LipE (1.23 vs 0.756). Replacement of methoxyphenyl of compound **9** with aminothiazole from compound **1** gave compound **10** with a 10-fold boost in potency, most likely due to forming a hydrogen bonding interaction with Val281. This modification also had a significant effect on improving the LipE (3.02) due to the lower lipophilicity of the aminothiazole vs the methoxyphenyl. A chlorine atom was introduced adjacent to the amide linkage in compound **10** in order to create torsional strain and mimic the expected binding conformation where the plane of the amide and pyridine are almost perpendicular. This modification further improved the potency by 25-fold and also LipE (3.7), giving the optimized compound **11**.

DOI: 10.1021/acs.jmedchem.7b00708
J. Med. Chem. XXXX, XXX, XXX−XXX

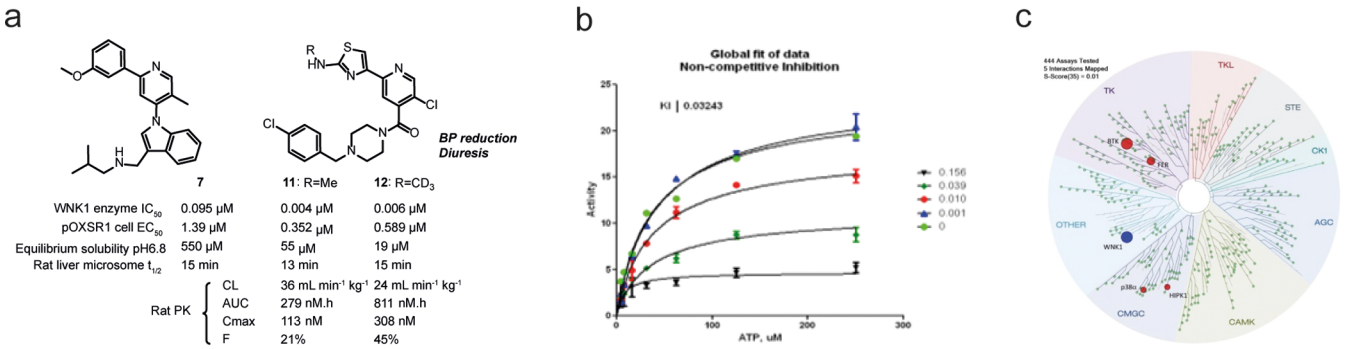

Figure 4. Profiles of optimized compounds. (a) *In vitro* profiles of optimized compounds **7**, **11**, and **12** and pharmacokinetics in Sprague–Dawley rats (0.5 mg kg^{-1} *i.v.*, 1.5 mg kg^{-1} *p.o.*) for compounds **11** and **12**. (b) Michaelis–Menten curves showing ATP noncompetitive binding for compound **4**. (c) Kinase selectivity data for compound **11** based on AMBIT KINOMEscan. Green dots indicate less than 35% inhibition, and red dots indicate greater than 35% inhibition at 10 μM screening concentration. Blue dot indicates on target activity. *Images generated using TREEspot Software Tool and reprinted with permission from KINOMEscan, a division of DiscoveRx Corporation; Copyright Discoverx Corporation 2010.

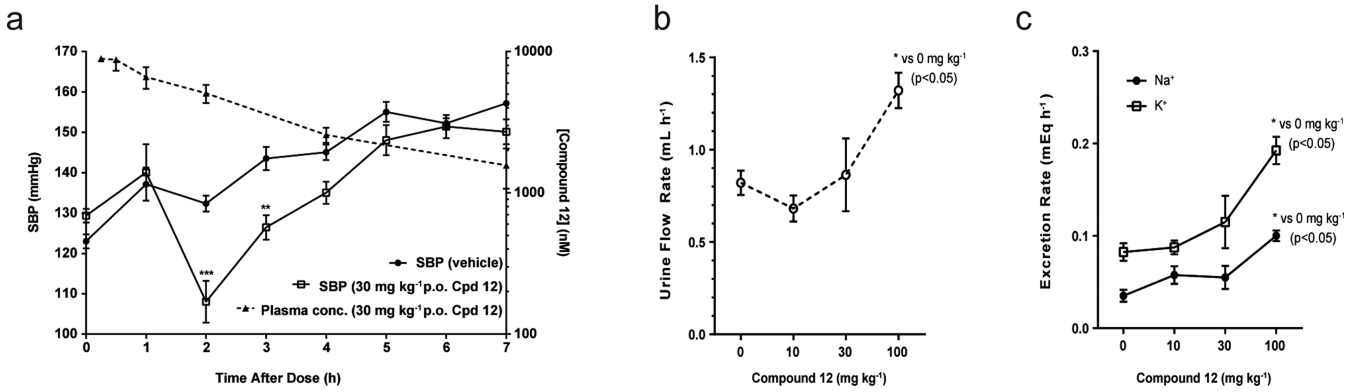

Figure 5. Pharmacokinetics and pharmacodynamics of compound **12**. (a) When dosed at 30 mg kg^{-1} *p.o.* in FVB mice overexpressing human WNK1, compound **12**-treated mice showed significant reductions in systolic blood pressure (SBP) vs untreated mice (time-weighted average, vs 24 h before treatment). In a separate cohort of mice dosed at 30 mg kg^{-1} *p.o.*, the plasma concentration reached nearly 10 μM at early time points and declined to approximately 1 μM after 7 h. Data in panel a show mean ± SEM, $n = 4$ per group for blood pressure studies, $n = 3$ for pharmacokinetic study; $^{**}p < 0.01$, $^{***}p < 0.001$ compared to vehicle (two-way analysis of variance (ANOVA) with Bonferroni post-test). (b,c) Compound **12** dose-dependently increased urinary volume (b) and urinary sodium and potassium excretion (c) in SHRs over a 7 h period. Data in panels b and c show mean ± SEM, $n = 4$ per group; $^{*}p < 0.05$ compared to vehicle (one-way analysis of variance (ANOVA) with Bonferroni post-test).

Compounds **7** and **11** showed $IC_{50} < 2$ μM in the cellular OSR1 phosphorylation assay with reasonable aqueous solubility, albeit with still rather high microsomal clearance (Figure 4a). Based on the overall lipophilic efficiency of compound **11** over **7**, we decided to further profile compound **11** for suitability for *in vivo* proof of concept study for allosteric WNK1 inhibition. Consistent with the allosteric mode of inhibition, compound **11** showed ATP noncompetitive inhibition (Figure 4b). When tested against a panel of 440 human kinases at 10 μM concentration, 2500-fold above enzyme IC_{50} value, compound **11** showed excellent selectivity with only a few significant off-target kinase inhibitions, most notably Burton's tyrosine kinase (BTK) and feline encephalitis virus-related (FER) kinase, neither of which are implicated for blood pressure regulation (Figure 4c, Table S1). This excellent selectivity profile is consistent with the predicted allosteric binding mode outside the highly conserved ATP-pocket (Figure 3c).

It was a fortuitous finding that compound **11** showed nearly 1000-fold selectivity for WNK1 vs WNK4 and 57-fold selectivity for WNK1 vs WNK2 (Figure S3a–d), providing an alternative tool compound to previously disclosed pan-WNK inhibitor WNK463.[3] During the optimization process, it was also observed that some compounds demonstrated high selectivity against WNK2 and WNK4 but never against WNK3. Our homology model supported this general observation that achieving selectivity within WNK family members is challenging, particularly for WNK3 where the residues surrounding the allosteric pocket were essentially identical with WNK1 (Figure S2b). For WNK2 and WNK4, there were some notable differences in the allosteric pocket, such as Phe in place of Ser286 and Val in place of Ala269, for WNK2 and WNK4, respectively (Figure S2a,c). However, beyond the fact that the selectivity seems to be affected by changes in the linker, which lies in proximity to the noted amino acid differences that are situated between the glycine rich loop and helix C, it remains to be determined how exactly compound **11** achieves the apparent selectivity over WNK4 or WNK2.

Based on the promising *in vitro* profiles, compound **11** was used for rat PK and showed moderate clearance but relatively low oral bioavailability and absolute exposure (Figure 4a, Table S1). Metasite[13,14] and StarDrop P450 analysis[15] both suggested *N*-demethylation as the major metabolic liability for compound **11**, and we had also noticed chemical stability issues for solutions of *N*-methylaminothiazole derivatives. We considered

DOI: 10.1021/acs.jmedchem.7b00708
J. Med. Chem. XXXX, XXX, XXX–XXX

a variety of replacements such as cyclopropyl for this methyl in analogous series to block metabolism, but all suffered from significant loss in potency. Deuteration has also been shown to improve pharmacokinetic profiles, due to the kinetic isotope effect,[16,17] so we explored the perdeuteromethyl analogue of compound **11** to assess whether this would provide sufficient improvement to enable *in vivo* PD/efficacy studies (Figure 4a). Compound **12** did show an improved rat PK profile, including lower clearance, improvement in absolute oral exposure, and a 2-fold improvement in oral bioavailability (Figure 4a, Table S1). Although we did not carry out full selectivity profiling with compound **12**, we had a high confidence that this would not change significantly vs compound **11**, and therefore, when dosed *in vivo*, the molecule would exert its effect via specific inhibition of WNK kinases and not be affected by off-target kinase inhibition.

In FVB mice overexpressing human WNK1 with implanted radiotelemetry devices,[3] single oral doses at 10, 30, and 100 mg kg^{-1} of compound **12** resulted in dose-dependent reductions in systolic blood pressure both in terms of peak and time-weighted average (TWA) vs baseline (Figure 5a, Table S2). The observed blood pressure reduction at 30 mg kg^{-1} coincided with a plasma exposure at or above ~2 μM (~3-fold above cellular IC_{50}) in a separate cohort of animals (Figure 5a). In another preliminary study, a single oral dose of 30 mg kg^{-1} of compound **7** resulted in a similar blood pressure reduction (Table S2), providing further evidence that allosteric inhibition of WNK kinase activities result in robust reduction in blood pressure.

To further understand the effect of allosteric WNK inhibitors on urinary output/electrolyte excretion and hemodynamic parameters, single ascending oral doses of compound **12** were given on successive days (vehicle, 10, 30, then 100 mg kg^{-1}) to spontaneously hypertensive rats (SHR) chronically instrumented with ascending aortic flow probes and aortic catheters/radiotransmitters for continuous recording of cardiac output and blood pressure.[18] Consistent with our previous findings on WNK1−4 kinase inhibition,[3] compound **12** induced dose-dependent diuresis, natriuresis, and kaliuresis, from 10 to 100 mg kg^{-1} (Figure 5b,c). While the observed diuresis and natriuresis were similar to that observed from a single oral dose of amiloride at 10 mg kg^{-1}, kaliuresis was observed only with the WNK inhibitor (Figure S5a,b), consistent with previously reported WNK physiology.[1,3] In terms of hemodynamic parameters, compound **12** showed trends toward reduction of blood pressure, stroke volume, and total peripheral resistance, while increasing heart rate (Figure S6a,b).

CONCLUSION

A dynamic morphing of three independent allosteric WNK1 inhibitors based on an overlay hypothesis and a docking model enabled an efficient optimization that led to the discovery of potent and selective allosteric inhibitors with improved physicochemical properties. Compound **12** showed efficacy in rodent models of hypertension and volume overload. Demonstration of both hemodynamic as well as renal effects of WNK1 inhibition through a different mode of binding than our previous report (allosteric vs ATP-site)[3] provides another line of evidence that the catalytic activity of WNK kinases play a fundamental role in cardiovascular homeostasis. One of the advantages of an allosteric binding site over the ATP-site for WNK inhibition is the potential to achieve selectivity among WNK family members such as for WNK1 vs WNK2 and WNK4. Topics of further investigation include the structural basis as well as functional and pharmacological consequences of such WNK family selectivity.

EXPERIMENTAL SECTION

The crystal structure of compound **1** bound to human WNK1 was disclosed previously (PDB 5TF9, purple ribbons). The crystal structures of compound **6** (PDB 5WDY, orange ribbons) and compound **8** (PDB 5WE8, green ribbons) were resolved independently utilizing the same human WNK1 construct and conditions as disclosed previously. Docking models in Figures 1c−f and 3c were created using the X-ray structure of compounds **1** and **8**, respectively, using Glide-SP v5.0 and MacroModel v9.6 (Schrödinger, LLC, New York). *In vitro* determination of WNK kinase catalytic activity utilized recombinant WNK kinase domains purified from *E. coli*. *In vitro* WNK kinase activity was assessed by a mobility shift assay of peptide substrate. Enzyme kinetics analyses were performed with GraphPad Prism for Windows version 7. WNK-mediated phosphorylation of exogenous OSR1 in HEK293 cells was shown by AlphaLISA. *In vivo* cardiovascular studies utilized telemetry to monitor blood pressure and heart rate in conscious WNK1 transgenic mice and aortic flow probes and aortic catheters/radiotransmitters to continuously record cardiac output and blood pressure in conscious SHRs. Metabolic cages were used for urine collection, and venous blood samples were collected for plasma electrolyte and pharmacokinetic analysis. LipE values were calculated with the formulas proposed by Ryckmans et al:[12] LipE = pIC_{50} − cLogP. A detailed summary of experimental procedures for the chemical synthesis, assays, and X-ray can be found in the Supporting Information.

Chemical Synthesis. Unless otherwise specified, all solvents and reagents were obtained from commercial sources and used without further purification. All reactions were performed under nitrogen atmosphere unless otherwise noted. Normal-phase flash chromatography was performed using Merck silica gel 60 (230−400 mesh). ^{1}H and ^{13}C NMR spectra were recorded on a Bruker DRX or a Bruker AV400 (400 MHz for ^{1}H and 100 MHz for ^{13}C). Chemical shifts are reported in parts per million (ppm) downfield from tetramethylsilane (0.00 ppm) or residual peaks from the corresponding solvent as an internal standard and coupling constants (J) in Hz. Multiplicity abbreviation are as follows: s = singlet, d = doublet, t = triplet, q = quartet, m = multiplet, app = apparent, br = broad. LC−MS analyses were performed on an HPLC system with a C18 column coupled to a single quad mass spectrometer with electrospray ionization (ESI). High-resolution mass spectra were obtained with Acquity Xevo G2 QTof system with UPLC (Acquity UPLC BEH C18 column, 2−98% acetonitrile in water with 0.1% formic acid) coupled to time-of-flight detection after electrospray ionization.

Chemical Stability. Methylaminothiazoles **10** and **11** showed decomposition in 10 mM DMSO stock solution if kept at room temperature over a prolonged (few months) period of time. Aliquots of the DMSO stock solutions were thus kept frozen for assays and periodically checked for purity by either WNK1 inhibition assay and/or LC−MS.

Chemical Purity. All compounds were checked for purity before assay by LC−MS and confirmed to have >95% purity.

Synthesis of Compounds 3−7. *1-([1,1′-Biphenyl]-3-yl)-1H-indole.* A mixture of 1*H*-indole (1 g, 8.54 mmol), K_3PO_4 (3.81 g, 17.93 mmol), and copper(I) iodide (0.081 g, 0.427 mmol) in toluene (10 mL) was purged with nitrogen for a few minutes, then 3-bromo-1,1′-biphenyl (1.71 mL, 10.3 mmol) and cyclohexane-1,2-diamine (0.209 mL, 1.71 mmol) were added. The reaction mixture was refluxed for 2 days. After it was cooled, hexane was added to the mixture. The resultant suspension was filtered through a short silica gel pad, and the filtrate was concentrated *in vacuo*. The residue was purified by silica gel flash chromatography to give 1-([1,1′-biphenyl]-3-yl)-1*H*-indole (420 mg, 18%). ESI-MS m/z: 270.3 $[M + H]^+$.

1-([1,1′-Biphenyl]-3-yl)-1H-indole-3-carboxaldehyde. To a solution of 1-([1,1′-biphenyl]-3-yl)-1*H*-indole (420 mg, 1.56 mmol) in DMF (10 mL) was added phosphorus oxychloride (0.174 mL, 1.87

DOI: 10.1021/acs.jmedchem.7b00708
J. Med. Chem. XXXX, XXX, XXX−XXX

mmol) dropwise at 0 °C. The resultant solution was allowed to stir at room temperature for 1 h, then poured onto crushed ice. The suspension was adjusted to pH 6 with 2 N aqueous NaOH solution with cooling. The crystalline product was collected by filtration and washed with water to give 1-([1,1′-biphenyl]-3-yl)-1*H*-indole-3-carbaldehyde (360 mg, 70%, 90% pure). ESI-MS *m*/*z*: 298.2 $[M + H]^+$.

*Compound **3**: 1-(1-([1,1′-Biphenyl]-3-yl)-1H-indol-3-yl)-N-(cyclohexylmethyl)methanamine.* To a mixture of 1-([1,1′-biphenyl]-3-yl)-1*H*-indole-3-carbaldehyde (130 mg, 0.393 mmol) in MeOH (2 mL) was added cyclohexylmethanamine (0.051 mL, 0.393 mmol). The resultant suspension was warmed to 50 °C with stirring, and THF (2 mL) was then added to give a solution. After the resultant solution was stirred for 30 min, sodium cyanoborohydride (41.2 mg, 0.590 mmol) was added. The reaction mixture was stirred at room temperature until the conversion was completed. One milliliter of 1 N HCl solution was added to the reaction mixture. The resultant mixture was stirred for 30 min, then adjusted to pH 8 with 1 N aqueous NaOH solution and diluted with water. The cloudy solution was extracted with dicholoromethane once. The extract was dried over Na_2SO_4 and concentrated. The residue was purified by silica gel flash chromatography, eluting with hexane/ethyl acetate (1:1) to give 1-(1-([1,1′-biphenyl]-3-yl)-1*H*-indol-3-yl)-*N*-(cyclohexylmethyl)-methanamine (91 mg, 59%). ^{1}H NMR (300 MHz, DMSO-d_6) δ ppm 7.80−7.33 (m, 12H), 7.25−7.05 (m, 2H), 3.88 (s, 2H), 2.45 (d, 2H), 1.83−1.52 (m, 5H), 1.42 (m, 1 H), 1.28−0.78 (m, 5H). ESI-MS *m*/*z*: 282.0 $[M - NC_7H_{15}]^+$.

*Compound **4**: 1-Cyclohexyl-N-((1-(3′-methoxybiphenyl-3-yl)-1H-indol-3-yl)methyl)methanamine (13 mg, 12%).* ^{1}H NMR (400 MHz, chloroform-*d*) δ 7.89−7.40 (m, 8H), 7.39−7.25 (m, 4H), 7.13−6.93 (m, 1H), 4.14 (s, 2H), 3.98 (s, 3H), 2.71 (d, *J* = 6.7 Hz, 2H), 2.01−1.54 (m, 6H), 1.47−0.93 (m, 5H). ESI-MS *m*/*z*: 312.2 $[M - NC_7H_{15}]^+$.

*Compound **5**: 1-Cyclohexyl-N-((1-(2-(3-methoxyphenyl)pyridin-4-yl)-1H-indol-3-yl)methyl)methanamine (19 mg, 13%).* ^{1}H NMR (400 MHz, methanol-d_4) δ 8.79−8.69 (m, 1H), 8.04 (s, 1H), 7.96 (d, *J* = 1.8 Hz, 1H), 7.86−7.74 (m, 2H), 7.62−7.49 (m, 3H), 7.48−7.27 (m, 3H), 7.02 (ddd, *J* = 8.2, 2.5, 0.9 Hz, 1H), 4.44 (s, 2H), 3.89 (s, 3H), 2.88 (d, *J* = 6.7 Hz, 2H), 1.88−1.59 (m, 6H), 1.36−0.92 (m, 5H). ESI-MS *m*/*z*: 426.4 $[M + H]^+$.

*Compound **6**: 1-Cyclohexyl-N-((6-fluoro-1-(2-(3-methoxyphenyl)-pyridin-4-yl)-1H-indol-3-yl)methyl)methanamine (40 mg, 62.5%).* ^{1}H NMR (400 MHz, chloroform-*d*) δ 8.68 (d, *J* = 6.06 Hz, 1 H), 7.85−7.95 (m, 2 H), 7.51−7.58 (m, 2 H), 7.43−7.47 (m, 3 H), 7.24−7.30 (m, 1 H), 7.09−7.15 (m, 1 H), 6.97 (dt, 1 H), 4.16 (s, 2 H), 3.93 (s, 3 H), 2.93 (d, 2 H), 1.63−1.85 (m, 6H), 1.12−1.32 (m, 3 H), 0.92−1.07 (m, 2 H). ESI-MS *m*/*z*: 444.4 $[M + H]^+$.

*Compound **7**: N-((1-(2-(3-Methoxyphenyl)-5-methylpyridin-4-yl)-1H-indol-3-yl)methyl)-2-methylpropan-1-amine (610 mg, 80%).* ^{1}H NMR (400 MHz, DMSO-d_6) δ 0.89 (d, *J* = 6.57 Hz, 6H), 1.67−1.78 (m, 1H), 2.16 (s, 3H), 2.43 (d, *J* = 6.57 Hz, 2H), 3.83 (s, 3H), 3.92 (s, 2H), 6.98−7.03 (m, 1H), 7.11−7.22 (m, 3H), 7.39 (t, *J* = 7.58 Hz, 1H), 7.52 (s, 1H), 7.69 (s, 1H), 7.70 (d, *J* = 10.11 Hz, 1H), 7.77 (d, *J* = 7.58 Hz, 1H), 7.95 (s, 1H), 8.74 (s, 1H). HRMS *m*/*z*: 400.2387 (M + H, $C_{26}H_{29}N_3O$, requires 400.2383).

Synthesis of Compounds 2, 8, and 9. *tert-Butyl 4-(2-(3-Methoxyphenyl)quinoline-4-carbonyl)piperazine-1-carboxylate.* A 50 mL flask was charged with 2-(3-methoxyphenyl)quinoline-4-carboxylic acid (200 mg, 0.717 mmol), *N*-boc-piperazine (160 mg, 0.860 mmol), 1-hydroxy-7-azabenzotriazole (49 mg, 0.359 mmol), *N*,*N*-dimethylformamide (2.1 mL), 1-(3-(dimethylamino)propyl)-3-ethylcarbodiimide hydrochloride (165 mg, 0.860 mmol), and *N*,*N*-diisopropylethylamine (0.150 mL, 0.860 mmol). The mixture was stirred at room temperature for 18 h, then diluted with water and extracted with diethyl ether. The combined organic fractions were washed with dilute aqueous hydrochloric acid followed by saturated aqueous sodium bicarbonate and brine, dried over magnesium sulfate, concentrated, and purified by silica gel chromatography (ethyl acetate−hexanes) to give *tert*-butyl 4-(2-(3-methoxyphenyl)-quinoline-4-carbonyl)piperazine-1-carboxylate as a colorless foam (395 mg, 881 mmol, quant). ^{1}H NMR (400 MHz, chloroform-*d*) δ ppm 1.46 (s, 9 H) 3.14−3.40 (m, 4 H) 3.56−3.70 (m, 2 H) 3.83−3.91 (m, 1 H), 3.93 (s, 3 H), 3.97−4.05 (m, 1 H), 7.44 (t, *J* = 7.96 Hz, 1 H), 7.54−7.62 (m, 1 H), 7.67−7.72 (m, 1 H), 7.74−7.83 (m, 4 H), 8.17−8.27 (m, 1 H). ESI-MS *m*/*z*: 448 $[M + H]^+$.

(2-(3-Methoxyphenyl)quinolin-4-yl)(piperazin-1-yl)methanone. To a 50 mL flask containing *tert*-butyl 4-(2-(3-methoxyphenyl)-quinoline-4-carbonyl)piperazine-1-carboxylate (365 mg, 0.815 mmol) was added methylene chloride (2 mL) and trifluoroacetic acid (2 mL). The mixture was stirred at room temperature for 18 h, concentrated under reduced pressure, suspended in 1 N aqueous sodium hydroxide, and extracted twice with methylene chloride. The combined organic fractions were dried over sodium sulfate, filtered, and concentrated to give (2-(3-methoxyphenyl)quinolin-4-yl)(piperazin-1-yl)methanone as a colorless foam (281 mg, 0.810 mmol, 99% yield). ^{1}H NMR (400 MHz, chloroform-*d*) δ ppm 2.69−2.78 (m, 2 H), 3.05 (t, *J* = 5.04 Hz, 2 H), 3.17−3.24 (m, 2 H), 3.81−3.91 (m, 1 H), 3.93 (s, 3 H), 3.96−4.07 (m, 1 H), 7.01−7.07 (m, 1 H), 7.44 (t, *J* = 7.81 Hz, 1 H), 7.58 (ddd, *J* = 8.31, 7.05, 1.26 Hz, 1 H), 7.70 (d, *J* = 8.56 Hz, 1 H), 7.74−7.80 (m, 3 H), 7.83 (d, *J* = 7.55 Hz, 1 H), 8.21 (d, *J* = 8.56 Hz, 1 H). ESI-MS *m*/*z*: 348 $[M + H]^+$.

*Compound **2**: (4-Benzylpiperazin-1-yl)(2-(3-methoxyphenyl)-quinolin-4-yl)methanone.* To a solution of (2-(3-methoxyphenyl)-quinolin-4-yl)(piperazin-1-yl)methanone (0.1 mmol, 37.4 mg) and *N*,*N*-diisopropylethylamine (0.15 mmol; 19.4 mg) in dichloromethane (1 mL) was added benzyl bromide (0.105 mmol, 18.0 mg). The reaction mixture was stirred for 5 h and then quenched with H_2O. The organic layer was extracted with dichloromethane, passed through a phase separator, and concentrated under reduced pressure. The residue was purified by silica gel column chromatography (eluent: dichloromethane/ethanol) to give (4-benzylpiperazin-1-yl)(2-(3-methoxyphenyl)quinolin-4-yl)methanone (34.5 mg, 79%). ^{1}H NMR (400 MHz, DMSO-d_6) δ ppm 2.2 (br s, 1H), 2.39 (br s, 1H), ~2.50 (br s, 1H, seen as shoulder on DMSO peak), 2.60 (br s, 1H), 3.13 (br s, 1H), 3.20 (br s, 1H), 3.51 (br s, 2H), 3.69 (br s, 1H), 3.89 (s, 3H), 3.94 (br s, 1H), 7.10 (dd, *J* = 8.1, 2.2 Hz), 7.25 (m, 1H), 7.31 (m, 3H), 7.48 (t, *J* = 7.9 Hz), 7.67 (t, *J* = 7.7 Hz), 7.79−7.90 (m, 4H), 8.14−8.15 (m, 2H). ^{13}C NMR (100 MHz, DMSO-d_6) δ ppm 41.1, 46.54, 52.74, 55.2, 61.64, 112.28, 115.48, 115.67, 119.62, 122.84, 124.51, 126.94, 127.38, 128.12, 128.75, 129.64, 129.88, 130.4, 137.69, 139.45, 143.35, 147.44, 155.52, 159.68, 165.57. HRMS *m*/*z*: 438.2168 (M + H, $C_{28}H_{27}N_3O_2$, requires 438.2182).

*Compound **8**: (R)-N-(1-(4-Chlorobenzyl)pyrrolidin-3-yl)-2-(3-methoxyphenyl)-N-methylquinoline-4-carboxamide (28 mg, 58%).* ^{1}H NMR (400 MHz, DMSO-d_6, 413 K) δ ppm 1.98 (m, 1H), 2.34 (br s, 1H), 2.81 (m, 2H), 3.00 (br s, 3H), 3.55 (m, 2H), 3.90 (s, 3H), 7.07 (dd, *J* = 2.6, 0.9 Hz, 0.5H), 7.09 (m, 0.5H), 7.28−7.31 (m, 4H), 7.44−7.46 (m, 1H), 7.59 (ddd, *J* = 8.2, 6.9, 1.2 Hz, 1H), 7.71 (dd, *J* = 8.4, 0.8 Hz, 1H), 7.78−7.81 (m, 3H), 7.89 (s, 1H), 8.12 (dt, *J* = 8.45, 0.92 Hz). ^{13}CNMR (100 MHz, DMSO-d_6) δ ppm 27.44, 27.57, 28.53, 28.93, 31.49, 51.48, 52.76, 52.92, 53.14, 55.28, 55.29, 55.31, 56.42, 56.65, 57.19, 58.12, 58.17, 58.41, 112.36, 112.45, 115.34, 115.44, 115.48, 115.7, 115.77, 119.68, 119.7, 119.75, 122.64, 122.98, 123, 124.36, 124.61, 124.68, 127.3, 127.43, 127.55, 128.18, 128.23, 129.7, 129.77, 129.95, 129.98, 130.02, 130.06, 130.11, 130.42, 130.52, 131.32, 131.35, 137.92, 137.97, 138.14, 139.58, 139.6, 139.61, 144.23, 144.32, 144.39, 147.51, 147.52, 147.57, 155.71, 159.78, 159.79, 166.89, 166.94, 167.26. HRMS *m*/*z*: 486.1932 (M + H, $C_{29}H_{28}ClN_3O_2$, requires 486.1948).

*Compound **9**: (4-(4-Cchlorobenzyl)piperazin-1-yl)(2-(3-methoxyphenyl)pyridin-4-yl)methanone (43 mg, 51%).* ESI-MS *m*/*z*: 422 $[M + H]^+$. ^{1}H NMR (400 MHz, chloroform-*d*) δ ppm 2.35−2.42 (m, 2 H), 2.50−2.57 (m, 2 H), 3.37−3.44 (m, 2 H), 3.51 (s, 2 H), 3.78−3.86 (m, 2 H), 3.90 (s, 3 H), 6.97−7.02 (m, 1 H), 7.20 (dd, *J* = 4.93, 1.39 Hz, 1 H), 7.23−7.26 (m, 2 H), 7.28−7.32 (m, 2 H), 7.39 (t, *J* = 7.96 Hz, 1 H), 7.52−7.56 (m, 1 H), 7.57−7.59 (m, 1 H), 7.67−7.72 (m, 1 H), 8.74 (d, *J* = 4.80 Hz, 1 H). ESI-MS *m*/*z*: 428 $[M + H]^+$.

Synthesis of Compound 10. *Methyl 2-(2-Bromoacetyl)-isonicotinate.* To a solution of methyl 2-acetylisonicotinate (1 g,

DOI: 10.1021/acs.jmedchem.7b00708
J. Med. Chem. XXXX, XXX, XXX−XXX

5.58 mmol) in acetic acid was added bromine (575 μL, 11.2 mmol) and hydrogen bromide in acetic acid (33 wt %, 144 μL) at room temperature. The mixture was stirred at room temperature overnight. The reaction mixture was concentrated *in vacuo*. The residue was basified with 1 N aqueous NaOH, and extracted with dichloromethane. The organic layer was concentrated *in vacuo*. The residue was purified by silica gel column chromatography (heptane/ethyl acetate) to give methyl 2-(2-bromoacetyl)isonicotinate (350 mg, 24%). ESI-MS *m/z*: 260.1 $[M + H]^+$.

Methyl 2-(2-(Methylamino)thiazol-4-yl)isonicotinate. To a solution of methyl 2-(2-bromoacetyl)isonicotinate (329 mg, 1.275 mmol) in methanol (10 mL) was added 1-methylthiourea (172 mg, 1.91 mmol) at room temperature. The mixture was stirred at 60 °C for 2 h. The reaction mixture was quenched with 15 mL of 1 N aqueous $NaHCO_3$, extracted with dichloromethane, and passed through phase separator. The organic solvent was removed *in vacuo*. The residue was purified by silica gel column chromatography (heptane/ethyl acetate) to give methyl 2-(2-(methylamino)thiazol-4-yl)isonicotinate (260 mg, 82%). ESI-MS *m/z*: 250.4 $[M + H]^+$.

2-(2-(Methylamino)thiazol-4-yl)isonicotinic Acid. To a solution of methyl 2-(2-(methylamino)thiazol-4-yl)isonicotinate (260 mg, 1.043 mmol) in methanol (10 mL) was added 1 N sodium hydroxide solution (8.34 mL) at room temperature. The mixture was stirred at 60 °C for 2 h. The organic solvent was removed *in vacuo*. The residue was acidified by the addition of 1 N HCl. The precipitate formed was collected and washed with water to give 2-(2-(methylamino)thiazol-4-yl)isonicotinic acid (194 mg, 79%). ESI-MS *m/z*: 236.3 $[M + H]^+$.

*Compound **10**: (4-(4-Chlorobenzyl)piperazin-1-yl)(2-(2-(methylamino)thiazol-4-yl)pyridin-4-yl)methanone.* A mixture of 2-(2-(methylamino)thiazol-4-yl)isonicotinic acid (2.1 mmol, 500 mg), 1-(4-chlorobenzyl)piperazine (3.2 mmol, 672 mg), (benzotriazol-1-yloxy)tris(dimethylamino)phosphonium hexafluorophosphate (3.19 mmol, 1.4 g) and triethylamine (8.5 mmol, 1.18 mL) in *N*-methylpyrrolidinone (15 mL) was stirred overnight at room temperature. The reaction mixture was quenched with H_2O and extracted three times with ethyl acetate. The combined organic layers were washed with brine, dried over Na_2SO_4, filtered, and concentrated under reduced pressure. Purification by reverse phase HPLC gave (4-(4-chlorobenzyl)piperazin-1-yl)(2-(2-(methylamino)thiazol-4-yl)-pyridin-4-yl)methanone (120 mg, 13%). ^{1}HNMR (400 MHz, DMSO-d_6) δ ppm 2.37−2.53 (m, 4H), 2.89 (d, J = 3.2 Hz, 3H), 3.35 (brs, 2H), 3.47−3.64 (m, 4H), 7.25 (d, J = 3.2 Hz, 1H), 7.36−7.40 (m, 5H), 7.67 (q, J = 3.2 Hz, 1H), 7.81 (brs, 1H), 8.61 (d, J = 3.2 Hz, 1H). ^{13}CNMR (100 MHz, DMSO-d_6); δ ppm 169.42, 166.79, 152.86, 149.64, 149.56, 144.08, 138.24, 131.54, 130.67, 128.16, 119.28, 117.45, 105.55, 60.50, 51.74, 46.61, 41.16, 30.81. ESI-MS *m/z*: 428.3 $[M + H]^+$.

Synthesis of Compound 11. *(4-(4-Chlorobenzyl)piperazin-1-yl)(2,5-dichloropyridin-4-yl)methanone.* A solution of 2,5-dichloroisonicotinic acid (3.0 g, 15.7 mmol) in thionyl chloride (15 mL) was refluxed for 2 h. After removal of solvents under reduced pressure, the residue was dissolved in dichloromethane (15 mL). Triethylamine (6.53 mL, 46.9 mmol) was added to the mixture followed by 1-(4-chlorobenzyl)piperazine (3.95 g, 18.8 mmol). The mixture was stirred for 2 h at room temperature before addition of water and dichloromethane. The organic layer was separated. The aqueous layer was extracted with dichloromethane. The combined organic layer was dried over Na_2SO_4, filtered, and concentrated under reduced pressure. The residue was purified by silica gel column chromatography (heptane/ethyl acetate) to give (4-(4-chlorobenzyl)piperazin-1-yl)(2,5-dichloropyridin-4-yl)methanone (5.5 g, 92%).

*Compound **11**: (5-Chloro-2-(2-(methylamino)thiazol-4-yl)-pyridin-4-yl)(4-(4-chlorobenzyl)piperazin-1-yl)methanone.* To a solution of (4-(4-chlorobenzyl)piperazin-1-yl)(2,5-dichloropyridin-4-yl)-methanone (790 mg, 2.05 mmol), and tributyl(1-ethoxyvinyl)tin (0.75 mL, 2.24 mmol) in 1,4-dioxane (20 mL) was added $Pd(PPh_3)_4$ (120 mg, 0.104 mmol), and the mixture was stirred at 100 °C for 20 h. After letting it cool to rt, the reaction mixture was poured into 2 M aqueous potassium fluoride solution (5 mL) and stirred for 2 h. To this reaction mixture was added *N*-bromosuccucinimide (400 mg, 2.25 mmol) in one portion. This reaction mixture was stirred for 2 h at rt. *N*-Methyl-thiourea (280 mg, 3.11 mmol) was added into the reaction mixture, which was stirred for 2 h. Insoluble material was removed by filtration, rinsing with dichloromethane. The organic extract was passed through an SCX column, which was rinsed with methanol and eluted with 20:2:1 EtOAc/MeOH/Et_3N. The crude material was purified by silica gel chromatography with ethyl acetate/methanol/triethylamine as coeluents to give (5-chloro-2-(2-(methylamino)-thiazol-4-yl)pyridin-4-yl)(4-(4-chlorobenzyl)piperazin-1-yl)methanone (700 mg, 64%). ^{1}HNMR (400 MHz, DMSO-d_6) δ ppm 2.92 (d, J = 11.2 Hz, 3H), 3.04 (brs, 2H), 3.18−3.20 (m, 1H), 3.28−3.30 (m, 1H), 3.35−3.43 (m, 2H), 3.49−3.67 (m, 2H), 4.33−4.41 (m, 2H), 4.56−4.61 (m, 1H), 7.41 (m, 1H), 7.54 (brs, 2H), 7.62−7.66 (m, 2H) 7.80 (brs, 1H), 7.88 (s, 1H), 8.69 (s, 1H), 11.56 (brs, 0.5H), 11.75 (brs, 0.5H). ^{13}CNMR (100 MHz, DMSO-d_6) δ ppm 169.50, 163.58, 163.40, 151.27, 151.10, 148.84, 148.01, 142.50, 142.31, 134.35, 133.31, 128.70, 128.35, 128.13, 124.63, 124.48, 118.45, 106.52, 57.71, 57.41, 50.56, 49.99, 49.86, 49.46, 42.88, 42.26, 39.91, 37.72, 30.91. HRMS (TOF) calcd. for $C_{21}H_{22}Cl_2N_5OS$ $[M + H]$ +462.0922, found 462.0933.

Synthesis of Compound 12. *tert-Butyl (4-(5-Chloro-6-(4-(4-chlorobenzyl)piperazine-1-carbonyl)pyridin-2-yl)thiazol-2-yl)-carbamate.* To a solution of (4-(4-chlorobenzyl)piperazin-1-yl)(2,5-dichloropyridin-4-yl)methanone (550 mg, 1.43 mmol) and tributyl(1-ethoxyvinyl)tin (0.5 mL, 1.487 mmol) in 1,4-dioxane (20 mL) was added $Pd(PPh_3)_4$ (70 mg, 0.061 mmol), and the mixture was stirred at 100 °C for 7 h. After letting it cool to rt, the reaction mixture was added into 2 M aqueous potassium fluoride solution (5 mL). To this reaction mixture was added *N*-bromosuccucinimide (300 mg, 1.69 mmol) in one portion. This reaction mixture was stirred for 30 min at rt. Insoluble material was removed via filtration, rinsing with methanol (3 × 20 mL). The resulting filtrate was cooled to 0 °C into which a solution of *N*-Boc-thiourea (400 mg, 2.27 mmol) was added. This reaction mixture was stirred for 2 h, letting warm it to rt. After removal of solvent, the resulting crude material was dissolved in dichloromethane and washed with 1 N aqueous NaOH solution and brine. The organic layer was dried over Na_2SO_4, filtered, and concentrated under reduced pressure. The residue was purified by silica gel column chromatography (heptane/ethyl acetate) to give *tert*-butyl (4-(5-chloro-6-(4-(4-chlorobenzyl)piperazine-1-carbonyl)pyridin-2-yl)-thiazol-2-yl)carbamate (550 mg, 70%). ^{1}H NMR (400 MHz, $CDCl_3$) δ ppm 1.58 (s, 9H), 2.40−2.46 (m, 2H), 2.56 (br s, 2H), 3.26−3.31 (m, 2H), 3.52 (s, 2H), 3.82−3.88 (m, 2H), 7.26−7.32 (m, 4H), 7.66 (s, 1H), 7.85 (s, 1H), 7.99 (br s, 1H), 8.59 (s, 1H). ESI-MS *m/z*: 548.0 $[M + H]^+$.

*Compound **12**: (5-Chloro-2-(2-((methyl-d_3)amino)thiazol-4-yl)-pyridin-4-yl)(4-(4-chlorobenzyl)piperazin-1-yl)methanone.* To a suspension of *tert*-butyl (4-(5-chloro-6-(4-(4-chlorobenzyl)piperazine-1-carbonyl)pyridin-2-yl)thiazol-2-yl)carbamate (530 mg, 0.966 mmol) and potassium carbonate (340 mg, 2.46 mmol) in DMF (15 mL) was added CD_3I (161 mg, 1.11 mmol) dropwise at 0 °C, and the mixture was stirred for 2 h letting warm to rt. After removal of the solvent under reduced pressure, the resulting material was suspended in water (50 mL) and stirred for 30 min at rt to form a brown precipitate. The resulting precipitate was collected via filtration and rinsed with cold water and hexane to give *tert*-butyl (4-(5-chloro-4-(4-(4-chlorobenzyl)piperazine-1-carbonyl)pyridin-2-yl)thiazol-2-yl)(methyl-d_3)carbamate (430 mg, 79%). ^{1}H NMR (400 MHz, $CDCl_3$) δ ppm 1.53 (s, 9H), 2.32−2.38 (m, 2H), 2.48 (br s, 2H), 3.18−3.27 (m, 2H), 3.43 (s, 2H), 3.70−3.72 (m, 1H), 3.82−3.86 (m, 1H), 7.17−7.23 (m, 4H), 7.64 (s, 1H), 7.92 (s, 1H), 8.49 (s, 1H). ESI-MS *m/z*: 565.4 $[M + H]^+$.

To a suspension of *tert*-butyl (4-(5-chloro-4-(4-(4-chlorobenzyl)-piperazine-1-carbonyl)pyridin-2-yl)thiazol-2-yl)(methyl-d_3)carbamate (50 mg, 0.088 mmol) in methanol (6 mL) was added 3 M aqueous HCl solution (0.3 mL, 0.90 mmol), and the mixture was stirred for 2 h at 60 °C. The mixture was cooled, and the solvent evaporated under reduced pressure gave compound **12**: (5-chloro-2-(2-((methyl-d_3)-amino)thiazol-4-yl)pyridin-4-yl)(4-(4-chlorobenzyl)piperazin-1-yl)-methanone hydrochloride (41 mg, 86%). ^{1}HNMR (400 MHz, DMSO-

DOI: 10.1021/acs.jmedchem.7b00708
J. Med. Chem. XXXX, XXX, XXX−XXX

d_6) δ ppm 3.04 (brs, 2H), 3.20 (brs, 1H), 3.29−3.42 (m, 3H), 3.52−3.62 (m, 2H), 4.35−4.40 (m, 2H), 4.59 (brs, 1H), 7.44 (brs, 1H), 7.54−7.55 (m, 2H), 7.63 (brs, 2H), 7.92−7.97 (m, 1H), 8.70 (s, 1H), 11.45 (brs, 0.5H), 11.58 (brs, 0.5H). ^{13}CNMR (100 MHz, DMSO-d_6) δ ppm 169.59, 163.73, 158.30, 158.05, 150.89, 148.86, 147.05, 142.48, 134.38, 133.29, 128.73, 124.91, 118.56, 116.16, 114.24, 106.65, 57.75, 50.58, 50.07, 49.93, 42.88, 42.34, 37.76, 30.71. HRMS (TOF) calcd. for $C_{21}H_{25}Cl_2N_5OS$ [M + H] +465.1156, found 465.1110.

■ ASSOCIATED CONTENT

Supporting Information

The Supporting Information is available free of charge on the ACS Publications website at DOI: 10.1021/acs.jmedchem.7b00708.

Detailed methods on protein production, purification, assay, and crystallization conditions (PDF)

Molecular formula strings and some data (CSV)

■ AUTHOR INFORMATION

Corresponding Author

* ken.yamada@novartis.com.

ORCID

Ken Yamada: 0000-0001-7899-6192

Upendra A. Argikar: 0000-0002-0939-0813

Present Addresses

[‖]J.L.: Constellation Pharmaceuticals, Cambridge, Massachusetts 02142, United States.

[⊥]T.Y.: Dong-A ST, Yongin, Gyeonggi 17073, Korea.

[□]D.F.R.: Rigel BioPharma Consulting LLC, Berkeley Heights, New Jersey 07922, United States.

[▽]K.D.: Insmed, Inc., Lake Hiawatha, New Jersey 07034, United States.

[○]M.Z.: Transamerica, 6 Rumbrook Road, Leominster, Massachusetts 01453, United States.

[◆]N.I.: Takeda Pharmaceuticals U.S.A., Inc., Cambridge, Massachusetts 02139, United States.

[⬢]Merck Research Laboratories, 33 Louis Pasteur Avenue, Boston, Massachusetts, 02115.

[¶]Y.I.Y.: FujiFilm Corporation, Kaiseimachi, Ashigarakami-gun, Kanagawa 258-8577, Japan.

[△]Y.I.: Janssen Pharmaceutical K.K., 2-5 Yarai-cho, Shinjuku, Tokyo 162-0805, Japan.

[▼]Z.R.: Short Path Distillery, Inc., 59 Magnolia Street, Arlington, Massachusetts 02474, United States.

Author Contributions

[#]These authors contributed equally to the work. T.Y., J.L., K.Yas., T.K., J.Y., L.M., Y.M., and H.I. designed and prepared the compounds, D.K. and X.X. performed X-ray crystallography, M.K. performed modeling, D.F.R., K.D.P., and L.X. designed and performed in vivo studies, Y.Y., P.T. and H.M.P. designed and performed mobility shift assays, D.Y., N.I., Y.Y., and H.M.P. designed and/or performed cellular OSR1 assays, U.A.A. and M.J. were responsible for pharmacokinetic studies, V.K. performed statistical analysis, and H.M.P. and K.Yam. directed the drug discovery program. All authors have given approval to the final version of the manuscript.

Notes

The authors declare the following competing financial interest(s): All authors were employed by Novartis Institutes for BioMedical Research during the period of their research described in this manuscript. All research was fully funded by Novartis.

■ ACKNOWLEDGMENTS

The authors thank Dr. Jason Elliott and Jovita Marcinkeviciene for their guidance in preparation of this manuscript and Drs. Genji Iwasaki, Lawrence Hamann, Jason Elliott, and Brian Jones for their guidance on medicinal chemistry strategy. The authors also thank the project team members Pramod Pandey, Jongchan Lee, and Chunhua Wang for protein production for biophysical and X-ray studies, Jessica Voltz for performing WNK1−4 mobility shift assays, Gang Zheng, Jey Jayaseelan, Jianning Ying, Sarah Mowbray, Waan-Jeng Huang, and Yang Luo for designing/performing cellular OSR1 assays, Lin Deng for performing PK studies, Tracy Herr for performing *in vivo* studies with human WNK1 transgenic mice, Fumin Fu, Jing Liu, Michael Beil, and Wei Chen for performing *in vivo* studies with SHR, and Karl Gunderson for NMR characterization.

■ ABBREVIATIONS USED

WNK, With-No-Lysine; ATP, adenosine triphosphate; AMP-PNP, adenylyl-imidodiphosphate; OSR1, oxidative-stress response 1; SPAK, STE20/SPS1-related proline/alanine-rich kinase; LipE, lipophilic efficiency

■ REFERENCES

(1) Wilson, F. H.; Disse-Nicodeme, S.; Choate, K. A.; Ishikawa, K.; Nelson-Williams, C.; Desitter, I.; Gunel, M.; Milford, D. V.; Lipkin, G. W.; Achard, J. M.; Feely, M. P.; Dussol, B.; Berland, Y.; Unwin, R. J.; Mayan, H.; Simon, D. B.; Farfel, Z.; Jeunemaitre, X.; Lifton, R. P. Human hypertension caused by mutations in WNK kinases. *Science* **2001**, *293*, 1107−1112.

(2) Mayan, H.; Vered, I.; Mouallem, M.; Tzadok-Witkon, M.; Pauzner, R.; Farfel, Z. Pseudohypoaldosteronism type II: marked sensitivity to thiazides, hypercalciuria, normomagnesemia, and low bone mineral density. *J. Clin. Endocrinol. Metab.* **2002**, *87*, 3248−3254.

(3) Yamada, K.; Park, H. M.; Rigel, D. F.; DiPetrillo, K.; Whalen, E. J.; Anisowicz, A.; Beil, M.; Berstler, J.; Brocklehurst, C. E.; Burdick, D. A.; Caplan, S. L.; Capparelli, M. P.; Chen, G.; Chen, W.; Dale, B.; Deng, L.; Fu, F.; Hamamatsu, N.; Harasaki, K.; Herr, T.; Hoffmann, P.; Hu, Q. Y.; Huang, W. J.; Idamakanti, N.; Imase, H.; Iwaki, Y.; Jain, M.; Jeyaseelan, J.; Kato, M.; Kaushik, V. K.; Kohls, D.; Kunjathoor, V.; LaSala, D.; Lee, J.; Liu, J.; Luo, Y.; Ma, F.; Mo, R.; Mowbray, S.; Mogi, M.; Ossola, F.; Pandey, P.; Patel, S. J.; Raghavan, S.; Salem, B.; Shanado, Y. H.; Trakshel, G. M.; Turner, G.; Wakai, H.; Wang, C.; Weldon, S.; Wielicki, J. B.; Xie, X.; Xu, L.; Yagi, Y. I.; Yasoshima, K.; Yin, J.; Yowe, D.; Zhang, J. H.; Zheng, G.; Monovich, L. Small-molecule WNK inhibition regulates cardiovascular and renal function. *Nat. Chem. Biol.* **2016**, *12*, 896−898.

(4) Huang, C. L.; Cheng, C. J. A unifying mechanism for WNK kinase regulation of sodium-chloride cotransporter. *Pfluegers Arch.* **2015**, *467*, 2235−2241.

(5) Uchida, S. Pathophysiological roles of WNK kinases in the kidney. *Pfluegers Arch.* **2010**, *460*, 695−702.

(6) Richardson, C.; Sakamoto, K.; de los Heros, P.; Deak, M.; Campbell, D. G.; Prescott, A. R.; Alessi, D. R. Regulation of the NKCC2 ion cotransporter by SPAK-OSR1-dependent and independent pathways. *J. Cell Sci.* **2011**, *124*, 789−800.

(7) Mori, T.; Kikuchi, E.; Watanabe, Y.; Fujii, S.; Ishigami-Yuasa, M.; Kagechika, H.; Sohara, E.; Rai, T.; Sasaki, S.; Uchida, S. Chemical library screening for WNK signalling inhibitors using fluorescence correlation spectroscopy. *Biochem. J.* **2013**, *455*, 339−345.

(8) Yamada, K.; Zhang, J. H.; Xie, X.; Reinhardt, J.; Xie, A. Q.; LaSala, D.; Kohls, D.; Yowe, D.; Burdick, D.; Yoshisue, H.; Wakai, H.; Schmidt, I.; Gunawan, J.; Yasoshima, K.; Yue, Q. K.; Kato, M.; Mogi, M.; Idamakanti, N.; Kreder, N.; Drueckes, P.; Pandey, P.; Kawanami, T.; Huang, W.; Yagi, Y. I.; Deng, Z.; Park, H. M. Discovery and characterization of allosteric WNK kinase inhibitors. *ACS Chem. Biol.* **2016**, *11*, 3338−3346.

DOI: 10.1021/acs.jmedchem.7b00708
J. Med. Chem. XXXX, XXX, XXX−XXX

(9) Fang, Z.; Grutter, C.; Rauh, D. Strategies for the selective regulation of kinases with allosteric modulators: exploiting exclusive structural features. *ACS Chem. Biol.* **2013**, *8*, 58−70.
(10) Dar, A. C.; Shokat, K. M. The evolution of protein kinase inhibitors from antagonists to agonists of cellular signaling. *Annu. Rev. Biochem.* **2011**, *80*, 769−795.
(11) Mobitz, H.; Jahnke, W.; Cowan-Jacob, S. W. Expanding the opportunities for modulating kinase targets with allosteric approaches. *Curr. Top. Med. Chem.* **2016**, *17*, 59−70.
(12) Ryckmans, T.; Edwards, M. P.; Horne, V. A.; Correia, A. M.; Owen, D. R.; Thompson, L. R.; Tran, I.; Tutt, M. F.; Young, T. Rapid assessment of a novel series of selective CB(2) agonists using parallel synthesis protocols: A lipophilic efficiency (LipE) analysis. *Bioorg. Med. Chem. Lett.* **2009**, *19*, 4406−4409.
(13) Cruciani, G.; Carosati, E.; De Boeck, B.; Ethirajulu, K.; Mackie, C.; Howe, T.; Vianello, R. MetaSite: understanding metabolism in human cytochromes from the perspective of the chemist. *J. Med. Chem.* **2005**, *48*, 6970−6979.
(14) Trunzer, M.; Faller, B.; Zimmerlin, A. Metabolic soft spot identification and compound optimization in early discovery phases using MetaSite and LC-MS/MS validation. *J. Med. Chem.* **2009**, *52*, 329−335.
(15) Tyzack, J. D.; Hunt, P. A.; Segall, M. D. Predicting regioselectivity and lability of cytochrome P450 metabolism using quantum mechanical simulations. *J. Chem. Inf. Model.* **2016**, *56*, 2180−2193.
(16) Harbeson, S. L.; Tung, R. D. Deuterium in drug discovery and development. *Annu. Rep. Med. Chem.* **2011**, *46*, 403−417.
(17) Uttamsingh, V.; Gallegos, R.; Liu, J. F.; Harbeson, S. L.; Bridson, G. W.; Cheng, C.; Wells, D. S.; Graham, P. B.; Zelle, R.; Tung, R. Altering metabolic profiles of drugs by precision deuteration: reducing mechanism-based inhibition of CYP2D6 by paroxetine. *J. Pharmacol. Exp. Ther.* **2015**, *354*, 43−54.
(18) Snelder, N.; Ploeger, B. A.; Luttringer, O.; Rigel, D. F.; Webb, R. L.; Feldman, D.; Fu, F.; Beil, M.; Jin, L.; Stanski, D. R.; Danhof, M. PKPD modelling of the interrelationship between mean arterial BP, cardiac output and total peripheral resistance in conscious rats. *Br. J. Pharmacol.* **2013**, *169*, 1510−1524.

DOI: 10.1021/acs.jmedchem.7b00708
J. Med. Chem. XXXX, XXX, XXX−XXX